Aftershocks of the Ridgecrest Earthquake Sequence and Their Relationship to Mainshock Slip and Scaling of Source Parameters

Final Technical Report of SCEC Award # 20073

Investigators: Taka'aki Taira (UC Berkeley), Douglas Dreger (UC Berkeley), and Jose Magana (UC Berkeley)

1. Project objectives

The connection between the strength of tectonic faults and the earthquake rupture is central to studies of the physics of earthquakes. Earthquake stress drop is one of source parameters for the earthquake rupture process that can be obtained from observed waveforms. The resultant stress drop could reflect the state of stress and the strength of the rocks in which the faulting occurs. Average stress drops are dependent on the mechanical model used to relate measured corner frequency to fault radius (e.g., Brune, 1970; Sato and Hirasawa, 1973; Madariaga, 1976). The differences in these models lead to more than a factor of 5 difference in estimated stress drop.

A finite-source based approach is not tied to a particular mechanical model and instead interprets observed moment rate function (MRF) in terms of the finite extent of slip given a typical rupture speed (a range of rupture velocities are typically examined to find the optimal fit). The finite source results (e.g., Dreger et al., 2007; Taira et al., 2015) show that for small earthquakes stable estimates of rupture area and therefore stress drop using the method of Ripperger and Mai (2004) may be determined.

We systematically investigate the earthquake stress drop for the Ridgecrest earthquake sequence through a finite-source modeling. This energetic earthquake sequence initiated early July 2019 and includes over 38,000 aftershocks listed in the Southern California Earthquake Data Center catalog (SCEDC, 2013). Thus far the Mw 6.4 foreshock was followed by the Mw 7.1 mainshock and over 950 M ≥ 3 aftershocks. Ross et al., (2019) report that much of the sequence occurred on a complex network of orthogonally oriented faults that were previously unknown. Resolving the spatial variation in earthquake stress drop will provide an additional constraint on the spatial distribution of locked asperity and will provide an improved understanding of the mechanics of the faulting process.

2. Methodology

We used empirical Green's functions, waveforms of nearly collocated smaller events, to correct for path, site and common elements in the source (focal mechanism) and recover an estimate of the seismic moment rate function (MRF). As shown in Mori and Hartzell (1990), these MRFs vary with azimuth from the source and carry information about the earthquake rupture directivity and the finite extent of the rupture. Ideally the magnitude difference between the target and

empirical Green's function is greater than one unit in moment magnitude to ensure that the small earthquake source corner frequency is well above that of the larger target event.

A smaller magnitude earthquake that satisfies these conditions is known as an empirical Green's function (eGf) event (Hartzell, 1978). The deconvolved moment rate functions are then inverted for slip (Mori and Hartzell, 1990; Dreger, 1994), testing the two possible double-couple nodal planes from the seismic moment tensor analysis, thereby finding the causative rupture plane of the earthquake. In this study, we aim to determine spatial-temporal source properties (source dimension, slip distribution, stress change, and rupture speed) for Mw < 6.0 events using moment-rate time histories of the source from empirical Green's function deconvolution.

3. Results

We comprehensively searched for possible eGf events for target earthquakes (with magnitude greater than 4.0) that occurred within 100km from the 2019 M7.1 Ridgecrest rupture area during the 2019-2020 period. A total of 148 earthquakes were analyzed as the target earthquakes. Using the SCEDC earthquake catalog (SCEDC, 2013), we searched for possible eGf events if events had 1) at least one magnitude unit smaller and 2) located within 5 km horizontally and 2 km vertically from target events.

For each eGf events, seismic waveforms from broadband sensors and accelerometers collected from stations were used to obtain the MRFs of target events with a frequency-domain water-level deconvolution (Clayton and Wiggins, 1976; Langston, 1979). A water level of 1% was used to stabilize the deconvolution procedure. We performed the deconvolution separately for each component and then stacked the three-component MRFs at each station to enhance signal-to-noise ratios (SNRs). We evaluated the quality of resultant MRFs based on resultant SNRs (Figure 1). If more than 10 stations exhibit their SNR higher than 15, we consider this eGf-target event pair for the finite-fault modeling.

The first event analyzed occurred on July 6, 2019 at 04:18:55 UTC in the northern part of the aftershock zone (Figure 2) of M 5.4. It is clear that good pulse-shaped Moment Rate Functions are obtained. We interpret the MRF by only considering the pulse with amplitude greater than zero to avoid potential side lobes of the spectral deconvolution. We tested both nodal-planes of the moment tensor solution and we find that the east-west striking has a slightly better fit of the data (Figure 3a).

Since the slip distribution is non-uniform, the method of Ripperger and Mai (2004) was done for the obtained MRF, the result yields an average stress drop of 20.7 MPa (Figure 3b). This is generally a high stress drop value and will be compared to other events of similar magnitudes. A jackknife analysis was performed to see if estimation results could be improved or if any station was a particulate outlier. We find that all the average slip distribution and average stress drops estimates varied within less than 5% from each other. We presented these results at the 2020 SCEC, 2020 AGU and 2021 SSA meetings (Magana et al., 2020). The second event analyzed was a Mw 4.6 aftershock that occurred on July 04, 2019. The resultant MRFs are generally well resolved and show a North-West directivity (Figure 4).

Additionally, to systematically explore characteristics of the rupture process for the Ridgecrest aftershocks, we determined the duration of MRFs for over 20 aftershocks (M>=4) and explored a scaling relation between Mw and duration. Our analysis suggests that the Brune stress drop model with a 10-MPa explains durations obtained in this study (Figure 5).

4. Reference

Brune, J. N., 1970, Tectonic stress and the spectra of seismic shear waves from earthquakes, J. Geophys. Res., 75, no. 26, 4997–5009.

Clayton, R. W., and R. A. Wiggins, 1976, Source shape estimation and deconvolution of teleseismic bodywaves, Geophys. J. Int., 47, no. 1, 151–177, doi: 10.1111/j.1365-246X.1976.tb01267.x.

Dreger, D. S., 1994, Northridge, California earthquake, Geophys. Res. Lett., 21, no. 24, 2633–2636, doi: 10.1029/94GL02661.

Dreger, D. S., R. M. Nadeau, and A. Chung, 2007, Repeating earthquake finite source models: Strong asperities revealed on the San Andreas Fault, Geophys. Res. Lett., 34, no. 23, L23302, doi: 10.1029/2007GL031353.

Hartzell, S. H., 1978, Earthquake aftershocks as Green's functions, Geophys. Res. Lett., 5, no. 1, 1–4, doi: 10.1029/GL005i001p00001.

Langston, C. A., 1979, Structure under Mount Rainier, Washington, inferred from teleseismic body waves, J. Geophys. Res., 84, no. B9, 4749, doi: 10.1029/JB084iB09p04749.

Madariaga, R., 1976, Dynamics of an expanding circular fault, Bull. Seismol. Soc. Am., 6, no. 3, 639–666.

Magana, J. A., Dreger, D. S., & Taira, T. (2020). Finite source modeling of the 2019 Ridgecrest aftershock sequence. Poster Presentation at 2020 SCEC Annual Meeting.

Mori, J., and S. Hartzell, 1990, Source inversion of the 1988 Upland, California, earthquake: Determination of a fault plane for a small event, Bull. Seismol. Soc. Am., 80, no. 3, 507–518.

Ripperger, J., and P. M. Mai, 2004, Fast computation of static stress changes on 2D faults from final slip distributions, Geophys. Res. Lett., 31, L18610, doi: 10.1029/2004GL020594.

Ross, Z. E. et al., 2019, Hierarchical interlocked orthogonal faulting in the 2019 Ridgecrest earthquake sequence, Science (80-.)., 366, 346–351.

Sato, T., and T. Hirasawa, 1973, Body wave spectra from propagating shear cracks, 415–431.

SCEDC, 2013, Southern California Earthquake Data Center, Caltech. Dataset, doi: 10.7909/C3WD3xH1.

Taira, T., D. S. Dreger, and R. M. Nadeau, 2015, Rupture process for micro-earthquakes inferred from borehole seismic recordings, Int. J. Earth Sci., 104, no. 6, 1499–1510, doi: 10.1007/s00531-015-1217-8.

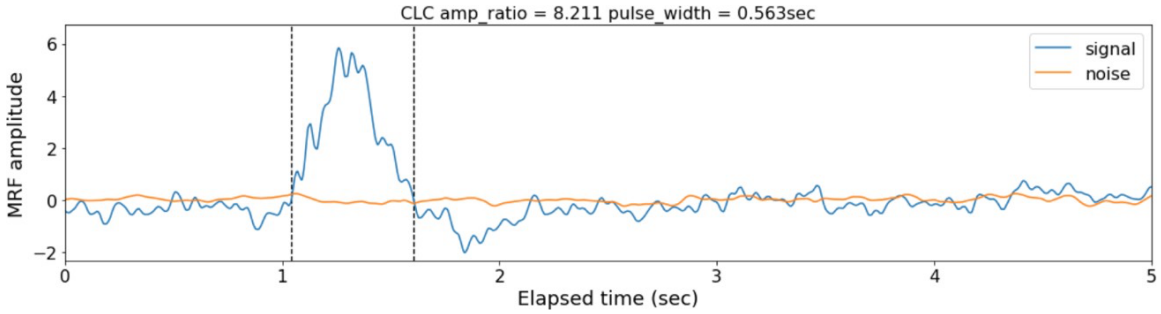

Figure 1. Example of MRF for the signal-to-noise ration evaluation and its pulse width measurement.

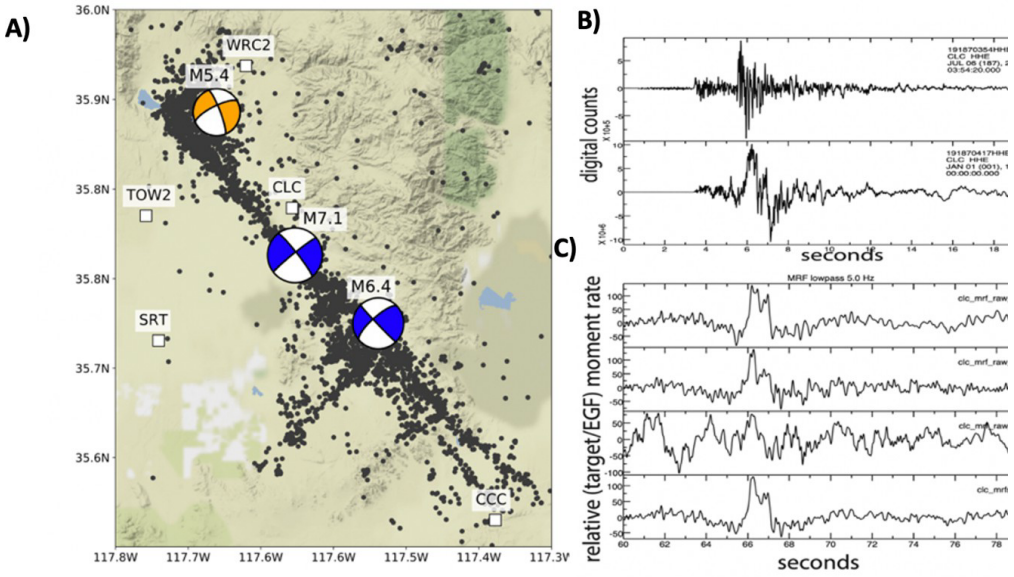

Figure 2. A) Location of the M 5.4 earthquake and the locations of nearby stations utilized in the inversion for this event. B) Waveforms for the target and eGf earthquakes. C) Resultant MRFs obtained separately for individual components. The bottom trace shows a stacked MRF.

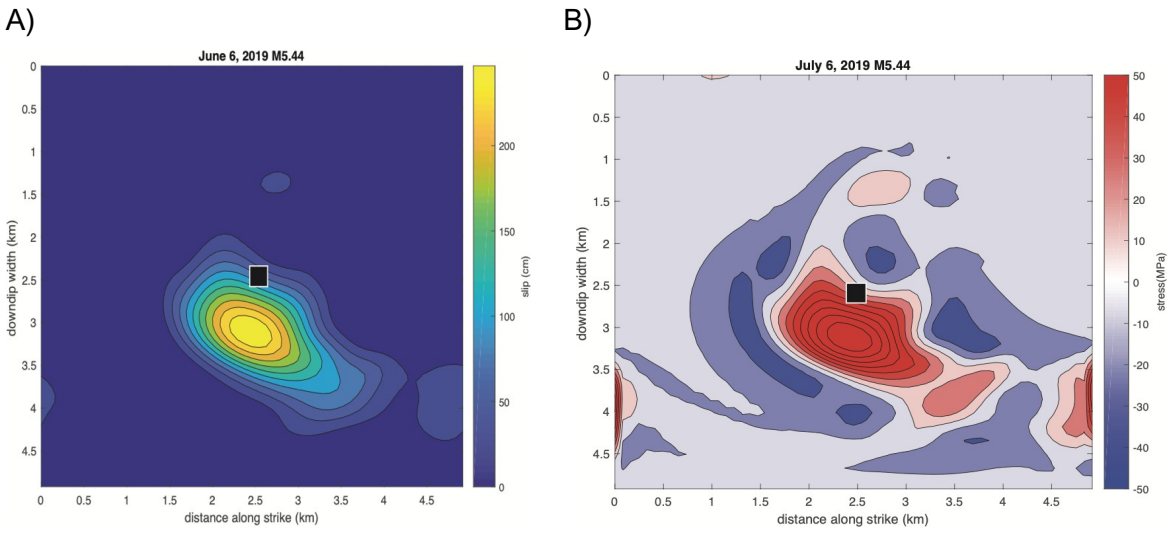

Figure 3. Spatial distributions of A) fault slip and B) stress drop for the 2019 Mw 5.44 Ridgecrest earthquake.

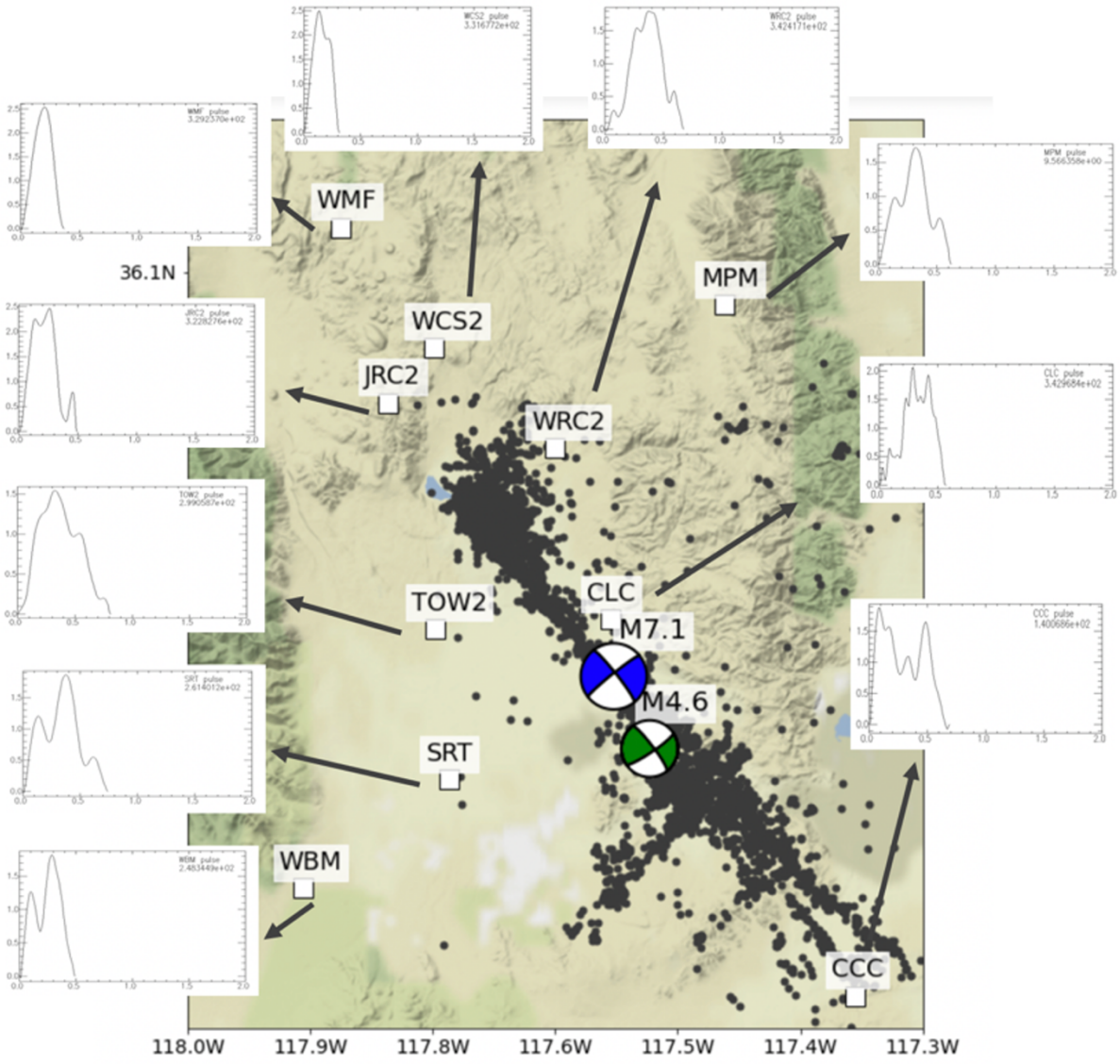

Figure 4. Location map of the Ridgecrest sequence, nearby broadband stations in the study area located with white squares. Image shows the location of one of the Mw 4.6 aftershock from July 04, 2019, and its focal mechanism (green) along with the focal mechanism of the Mw 7.1 mainshock (blue). Four months of aftershocks (gray dots) from the SCSN catalog within 50 km of the mainshock epicenter show complexity of the ruptured faults. Each station has its respective Moment Rate Function used in the finite-source inversion.

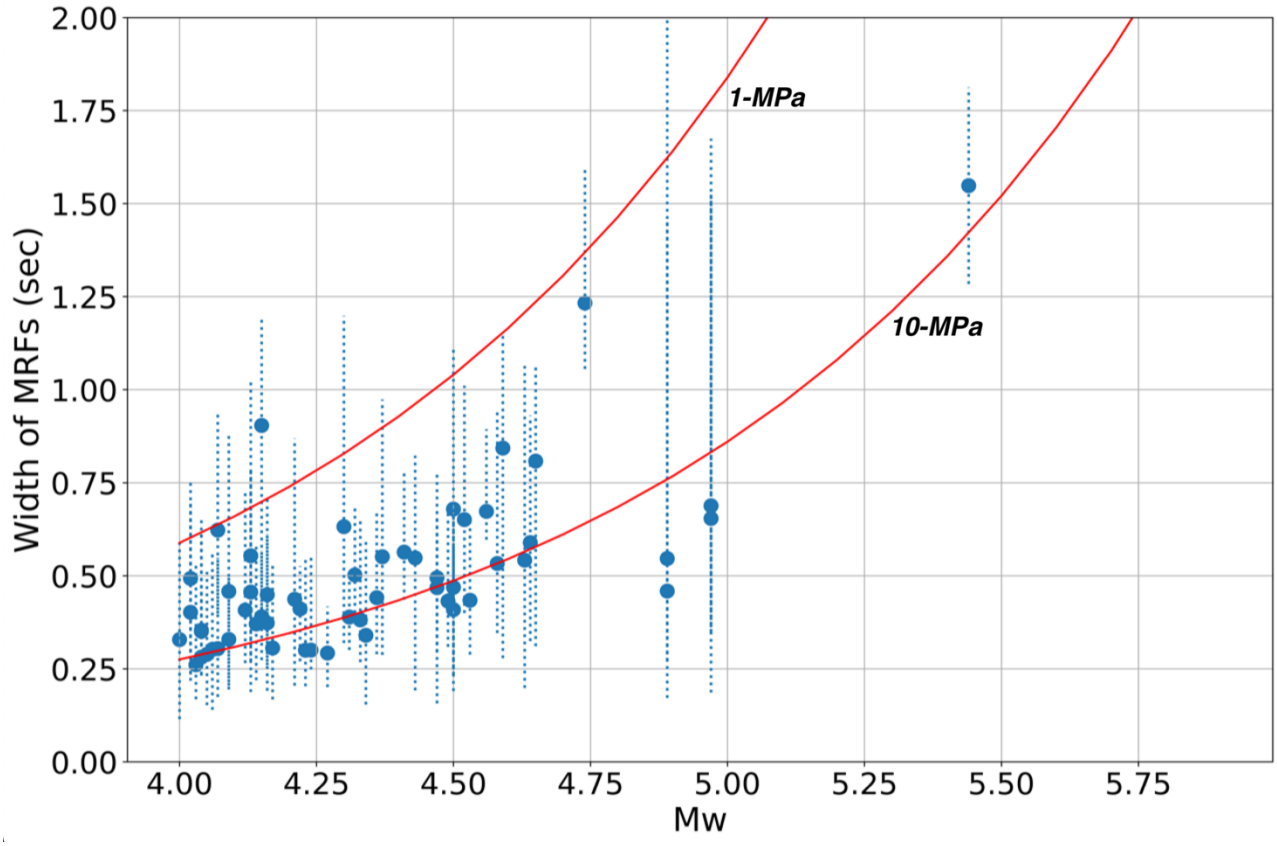

Figure 5. Duration of average MRFs obtained for Ridgecrest aftershocks. Average MRFs are obtained by stacking all available MRFs per event. Dashed lines show standard deviation. Two red lines show theoretical duration of MRFs based on the Brune stress drop model with 1-MPa and 10-MPa.